STRUCTURAL CONTROL AND HEALTH MONITORING
Struct. Control Health Monit. (2011)
Published online in Wiley Online Library (wileyonlinelibrary.com). DOI: 10.1002/stc.437

Direct adaptive neural controller for the active control of earthquake-excited nonlinear base-isolated buildings

Sundaram Suresh[1,‡], Sriram Narasimhan[2,*,†,‡] and Satish Nagarajaiah[3,§]

[1]*School of Computer Engineering, Nanyang Technological University, Singapore*
[2]*Departmant of Civil and Environmental Engineering, 200 University Avenue West, University of Waterloo, Waterloo, Ontario, Canada*
[3]*Civil and Environmental Engineering and Mechanical and Materials Engineering, Rice University, TX, U.S.A.*

SUMMARY

This paper presents a nonlinearly parameterized controller for the adaptive control of base-isolated buildings subjected to a set of near-fault earthquakes. The control scheme is based on discrete direct adaptive control, wherein the system response is minimized under parameter uncertainties. Stable tuning laws for the controller parameters are derived using the Lyapunov approach. The controller utilizes a linear combination of nonlinear basis functions, and estimates the desired control force online. The measurements that are necessary to generate the control force to reduce the system responses under earthquake excitations are developed based on the adaptive systems theory. The main novelty in this paper is to approximate the nonlinear control law using a nonlinearly parameterized neural network, without an explicit training phase. A perturbed model is used to initialize the controller parameters in order to simulate the uncertainty in the mathematical modeling that typically exists in representing civil structures. Performance of the proposed control scheme is evaluated on a full-scale nonlinear three-dimensional (3-D) base-isolated benchmark structure. The lateral-torsion superstructure behavior and the bi-axial interaction of the nonlinear bearings are incorporated. The results show that the proposed controller scheme can achieve good response reductions for a wide range of near-fault earthquakes, without a corresponding increase in the superstructure response. Copyright © 2011 John Wiley & Sons, Ltd.

Received 30 May 2010; Revised 21 November 2010; Accepted 22 November 2010

KEY WORDS: active control; base isolation; adaptive systems; neural networks

INTRODUCTION

Structural control has gained significant attention as an effective means to reduce structural vibrations due to imposed dynamic forces such as wind and earthquakes [1,2]. Various control methodologies and devices have been proposed in the literature for this purpose, and the volume of this activity does not permit a comprehensive review of the pertinent literature. The main idea of this paper is to present a new adaptive controller that is robust to the uncertainties in the structure parameters, and applicable to nonlinear base-isolated buildings. This research is motivated by the need to restrict the large displacements at the isolation layer caused by

*Correspondence to: Sriram Narasimhan, Department of Civil and Environmental Engineering, 200 University Ave. W., University of Waterloo, Waterloo, Ontario, Canada.
†E-mail: snarasim@uwaterloo.ca
‡Assistant Professor.
§Professor.

near-fault earthquakes, while retaining the advantages gained by lengthening of the natural period of the structure [3,4].

The idea behind base-isolation is to lengthen the natural period of the structure, thereby shifting the dominant response mode during earthquakes to the low frequency regions of the spectrum where the energy contained in earthquakes is expected to be small. It is now widely accepted that the performance of base-isolated buildings (measured using indices such as accelerations and story-drifts) is superior to those (buildings) with fixed-base counterparts. However, this increased performance is achieved at the cost of increased isolation layer displacements, which may result in isolator instabilities, pounding, etc. In order to retain the benefits of base-isolation, several control strategies have been proposed in the literature [1]. The basic idea behind these approaches is to place control devices in the isolation layer that enhance the overall performance of the base-isolated structure, while retaining the fundamental characteristics of base-isolation.

Broadly speaking, there are three main structural control methodologies: passive, active and semiactive. As the name implies, passive control methods employ devices that are primarily variations or adaptations of traditional spring and viscous elements. Once deployed, these elements react to the forces imposed upon them, and there are no provisions to adapt them online. On the other hand, semiactive and active control strategies employ specialized hardware and algorithms to enable adaptation. Hydraulic actuators, electric motors, etc., are generally employed within the active control setting, whereas magneto-rheological dampers, variable-stiffness devices, etc., in semiactive control. The relative merits and de-merits of using active devices versus semiactive counterparts have been documented extensively in the literature [1].

The motivation to study active control as the test-bed for algorithmic development is as follows. A large number of the control algorithms used for semiactive and active control strategies are fundamentally the same, with the primary difference being the methodology used to operate the device itself. Whereas, the desired control force can be directly commanded using an active device by accounting for the actuator dynamics, this is not as straight-forward in a semiactive device. For example, the desired control force needs to be converted into a current that can be commanded to the semiactive device using an inverse dynamic model of the device. However, from an algorithmic point of view, the underlying algorithms to calculate the force can be extended to work with semiactive devices as well [5,6], assuming that the semiactive device dynamics are known *a priori* or estimated online. Furthermore, the results from active control are often used as an upper-bound to evaluate the effectiveness of semiactive control strategies. The motivation for this study stems from this background, and it is expected that the control algorithm presented here can be extended, for instance, using a clipped approach-to semiactive control using, say, MR dampers.

Popular methods for the active control of base-isolated structures include linearization, sliding mode control [5,7,8] and adaptive control [9]. While both linear methods and nonlinear methods (such as sliding mode control) have provided excellent control designs, the need to control uncertain and fault-tolerant nonlinear systems has sparked an interest in adaptive control, especially using artificial neural networks (ANNs). ANNs have been used extensively for both structural system identification and control [10–22]. In many of these studies, especially the earlier ones involving control [12–14], the architecture consists of an identification phase and a control phase, which means that the quality of the controller is directly linked to the quality of the identifier. Subsequent studies [15–17] have investigated the application of NNs for linear structures without an identifier (called emulator), while retaining learn-then-control approach. In this paper, a new direct adaptive controller employing nonlinearly parameterized basis functions is presented. The tuning laws for the parameters are developed based on the adaptive systems theory. It will be shown that the resulting controller is robust to system parameter uncertainties and does not require the desired control output, which is cumbersome to obtain, for controller development.

A large body of literature on neuro-adaptive control exists on nonlinear systems of the form $\dot{x} = f(x)+g(x)u$, where the NNs are used to approximate $f(x)$ and $g(x)$ [23]. Adaptive control methods such as adaptive feedback linearization and back-stepping have been shown to be very

DOI: 10.1002/stc

effective for the control of a broad class of systems [9,24–29]. In contrast, in this paper, the function approximation capabilities of nonlinearly parameterized NNs are exploited to approximate a nonlinear control law. The adaptive controller is capable of handling uncertainties in both the system parameters and the nonlinear force estimation. The controller parameters are updated online, and the update laws are derived using the well-established Lyapunov approach. Unlike classical approaches using NNs where a formal identification phase precedes the controller development, there is no need for the identification in the current approach, which is its main advantage.

Numerical simulations are performed on a full-scale numerical test-bed base-isolated building [30] with an isolation system comprising hysteretic lead-rubber bearings (LRBs). The structure is excited simultaneously in two directions using a suite of severe near-fault earthquakes. The earthquakes considered in this study are: fault-normal (FN) and fault-parallel (FP) components of Newhall, Sylmar, El Centro, Rinaldi, Kobe and Erzinkan. The performance of the controller is measured using a comprehensive set of eight performance indices. These performance indices are chosen such that they reflect the relative trade-offs that exist between various response quantities that typically accompany a control scheme [30]. All the excitations are used at the full intensity for the evaluation of the performance indices.

SIMULATION MODEL OF THE BASE-ISOLATED STRUCTURE

The overall schematics of the base-isolated structure is shown in Figure 1. This structure is based on a full-scale structure located in Los Angeles, U.S.A. [30]. The superstructure is assumed to remain in the linear-elastic regime, while the nonlinearities in the isolation system provide for the energy dissipation. The asymmetry in the plan causes the structure to contain significant torsional components in addition to the lateral components. A Finite-Element (FE) model of the super-structure was constructed in the commercial FE program ETABS, which was then reduced to 24 degrees of freedom (24DOF) at the centers of mass of the eight floor

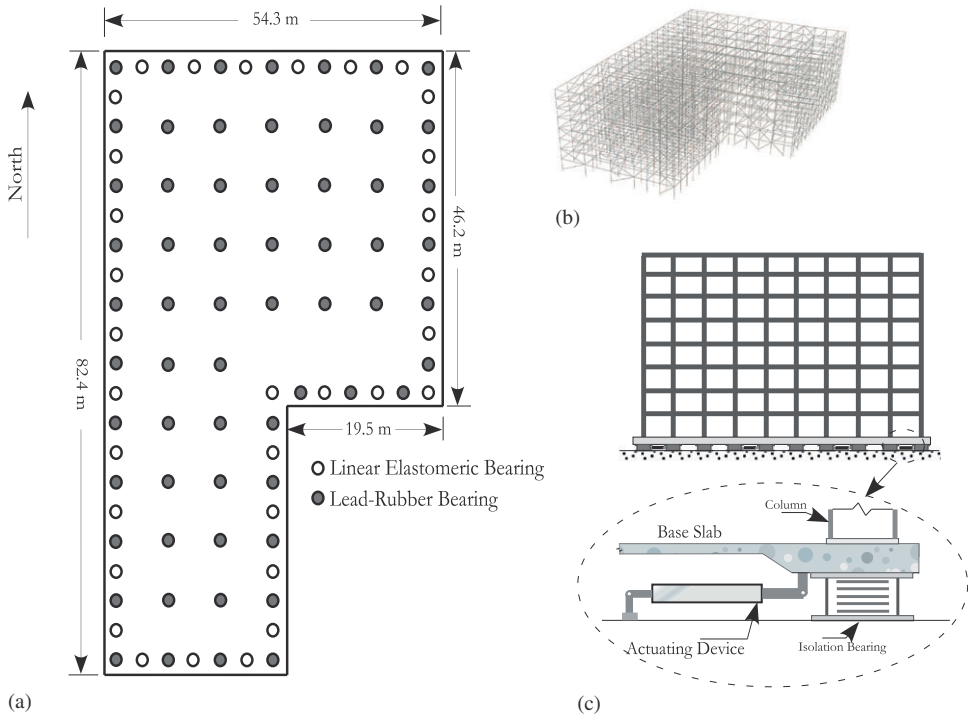

Figure 1. (a) Elevation view of the eight-story base-isolated building; (b) FE model; and (c) Typical actuator placement detail.

DOI: 10.1002/stc

levels. The isolation system model was then integrated into the reduced super-structure model for the ensuing simulations. While the isolation system exhibits hysteresis, the superstructure is assumed to dissipate the vibration energy due to viscous damping (assumed to be 5% in all modes). The details of this structure has been documented elsewhere [19,30], and not repeated here for the sake of brevity.

The combined equations of the linear superstructure and the base can be described as follows:

$$\mathbf{M}\ddot{\mathbf{U}}+\mathbf{C}\dot{\mathbf{U}}+\mathbf{K}\mathbf{U}+\mathbf{M}\mathbf{R}(\ddot{\mathbf{U}}_g+\ddot{\mathbf{U}}_b)=0 \tag{1}$$

$$\mathbf{R}^{\mathrm{T}}\mathbf{M}[(\ddot{\mathbf{U}})+\mathbf{R}(\ddot{\mathbf{U}}_g+\ddot{\mathbf{U}}_b)]+\mathbf{M}_b(\ddot{\mathbf{U}}_g+\ddot{\mathbf{U}}_b)+\mathbf{C}_b\dot{\mathbf{U}}_b+\mathbf{K}_b\mathbf{U}_b+\mathbf{f}_b(\mathbf{U}_b,\dot{\mathbf{U}}_b)+\mathbf{f}_c=0 \tag{2}$$

where $\mathbf{M}$ is the superstructure mass matrix, $\mathbf{M}_b$ is the diagonal mass matrix of the rigid base, $\mathbf{C}$ is the superstructure damping matrix, $\mathbf{C}_b$ is the resultant damping matrix of viscous isolation elements, $\mathbf{K}$ is the superstructure stiffness matrix, $\mathbf{K}_b$ is the resultant stiffness matrix of elastic isolation elements and $\mathbf{R}$ is the matrix of earthquake influence coefficients. Furthermore, $\ddot{\mathbf{U}}$, $\dot{\mathbf{U}}$ and $\mathbf{U}$ represent the floor acceleration, velocity and displacement vectors relative to the base, $\ddot{\mathbf{U}}_b$ is the vector of base accelerations relative to the ground and $\ddot{\mathbf{U}}_g$ is the vector of ground accelerations. $\mathbf{f}_b$ is the vector containing the nonlinear bearing forces, and $\mathbf{f}_c$ is the vector containing the control forces.

A mix of 31 linear elastic elastomeric bearings (with assumed viscous damping) and 61 hysteretic LRBs are assumed to constitute the isolation system. The evolution of hysteresis in the LRBs is modeled using the following nonlinear differential equations [4]:

$$\begin{gathered} U^y\begin{Bmatrix}\dot{z}_x\\ \dot{z}_y\end{Bmatrix}=\alpha\begin{Bmatrix}\dot{U}_{bx}\\ \dot{U}_{by}\end{Bmatrix}-\mathbf{Z}_w\begin{Bmatrix}\dot{U}_{bx}\\ \dot{U}_{by}\end{Bmatrix} \\ \mathbf{Z}_w=\begin{bmatrix} z_x^2(\gamma\,\mathrm{sgn}(\dot{U}_{bx}z_x)+\beta) & z_xz_y(\gamma\,\mathrm{sgn}(\dot{U}_{by}z_y)+\beta)\\ z_xz_y(\gamma\ \mathrm{sgn}(\dot{U}_{bx}z_x)+\beta) & z_y^2(\gamma\,\mathrm{sgn}(\dot{U}_{by}z_y)+\beta)\end{bmatrix}\end{gathered} \tag{3}$$

where z_x and z_y are dimensionless hysteretic variables which are bounded by values ± 1. α, β and and γ are dimensionless quantities and U^y is the yield displacement. The forces, f, mobilized in the elastomeric isolation bearings or devices (in the x and y directions) are modeled by a elastic-viscoplastic model with strain hardening, as follows:

$$f_x=k_pU_{bx}+c_v\dot{U}_{bx}+(k_e-k_p)U^yz_x \tag{4}$$

$$f_y=k_pU_{by}+c_v\dot{U}_{by}+(k_e-k_p)U^yz_y \tag{5}$$

where k_e is the pre-yield stiffness, k_p is the post-yield stiffness, c_v is the viscous damping coefficient of the elastomeric bearing or device, U^y is the yield displacement. The isolation system parameters have been specified in the following papers [6,7,30]. The readers are referred to the benchmark definition paper [30] for discussion on the solution procedure.

ADAPTIVE CONTROLLER DEVELOPMENT

The equations for the state for the base and the superstructure in discrete-time framework can be written as (shown earlier in Equations (1)–(5)):

$$\mathbf{z}(k+1)=f_1(\mathbf{z}(k),\boldsymbol{\eta}(k))+\mathbf{G}_1\mathbf{F}_c(k)+\mathbf{G}_1\mathbf{A}_g(k) \tag{6}$$

$$\boldsymbol{\eta}(k+1)=f_2(\mathbf{z}(k),\boldsymbol{\eta}(k))+\mathbf{G}_2\mathbf{A}_g(k) \tag{7}$$

where $\mathbf{A}_g(k)$ are the earthquake accelerations, $[\mathbf{z}(k)\ \boldsymbol{\eta}(k)]^{\mathrm{T}}\in\Omega_x\subset\Re^n$are the states of the discrete-time system corresponding to the base and the superstructure respectively on the compact set Ω_x, where $(\Omega_x:=\{\mathbf{z},\boldsymbol{\eta},\|\mathbf{z}\|\leqslant M_z;\|\eta\|\leqslant M_{\boldsymbol{\eta}}\})$, M_z, M_η are positive constants, and $\mathbf{F}_c\in\Omega_u\subset\Re^m$ are the actuator inputs on the compact set Ω_u, $(\Omega_u:=\{\mathbf{u},\|\mathbf{u}\|\leqslant M_u\})$, where M_u is a positive constant. $\mathbf{G}_1$ and $\mathbf{G}_2$ are the discrete-time control matrices.

DOI: 10.1002/stc

The functions f_1 and f_2 are smooth nonlinear functions. By assuming that the zero dynamics of $f_2(0, \boldsymbol{\eta}(k))$ is asymptotically stable, the control objective is to determine the bounded control input $\mathbf{F}_c^*$, such that the structural responses of the base $\mathbf{z}(k)$ follows the desired response $\mathbf{z}_d(k)$, i.e.

$$\|\mathbf{z}(k) - \mathbf{z}_d(k)\| \leqslant \epsilon \tag{8}$$

where ε is a small positive constant. It is also assumed that the function $f_1(\mathbf{z}, \boldsymbol{\eta})$ has continuous bounded partial derivatives in a certain neighborhood of all points along the desired response. Determining the conditions under which the desired control $\mathbf{F}_c^*$(note that $*$ represents the desired quantity) exists is the theoretical control problem. The significance of the assumption regarding zero dynamics is evident from Equation (8). Since the control tracking problem (and the error dynamics to be derived later) considering Equation (8) contains only partial states corresponding to the base, the stability of the overall system must take the entire state space into account. For structural systems with non-zero dissipative damping, the assumption of zero-dynamics made earlier is indeed valid.

Under the above assumptions, it follows from implicit function theorem [25,31] that there exists a desired control force F_c^*:

$$F_c^*(k) = \bar{\mathcal{G}}_1(F_c^*(k-1), \ldots, F_c^*(k-n), \mathbf{z}(k-1), \ldots, \mathbf{z}(k-n), \mathbf{A}_g(k), \ldots, \mathbf{A}_g(k-n), \mathbf{z}_d(k) \tag{9}$$

where $\bar{\mathcal{G}}_1$ is a smooth nonlinear map and n is the number of delays. The number of delays depends on the order of the system. The above form of control law is known to exist, and is unique [25,32]. If the structural response follows the desired response, then the signal from $F_c^*(k-1), \ldots, F_c^*(k-n)$ can be expressed in terms of the reference outputs and structural responses. Also, if the desired response is assumed to be near zero, then Equation (9) can be simplified further as:

$$F_c^*(k) = \bar{\mathcal{G}}(\mathbf{z}(k-1), \ldots, \mathbf{z}(k-n_1), \mathbf{A}_g(k), \ldots, \mathbf{A}_g(k-n_1)) \tag{10}$$

where $n_1 \geqslant n$. The above equation can be written as,

$$F_c^*(k) = \bar{\mathcal{G}}(\mathbf{v}) \tag{11}$$

where $\mathbf{v}$ consists of past states and present and past values of the ground accelerations. Equation (10) indicates if the mapping $\bar{\mathcal{G}}$ is known, then the desired control force $F_c^*(k)$ can be calculated using n_1 past values $\mathbf{z}$, and n_1+1 current and past values of the earthquake disturbance (define $l = 2n_1+1$). Since the function map $\bar{\mathcal{G}}$ is unknown, estimating the control force $F_c^*(k)$ is not possible. However, since the relationship given by Equation (10) exists, $\bar{\mathcal{G}}$ can be modeled using a nonlinearly parameterized NN. Note that for notational convenience, the discrete-time k in the ANN parameters is ignored.

The control law given in Equation (10) is approximated using a linear combination of h^* nonlinearly parameterized functions, each represented by the symbol σ. Mathematically stated,

$$F_c^*(k) = \sum_{i=1}^{h^*} \alpha_i^* \sigma\left(\sum_{j=1}^{l} w_{ij}^* v_j\right) \tag{12}$$

where $\mathbf{v} \in \Re^{l\times 1}$ is the input to the controller, the nonlinear function $\sigma : \Re^{h^*} \to \Re^{h^*}$ is continuous with respect to its arguments for all finite ($\mathbf{W}$, $\mathbf{v}$), and the adjustable parameters of the controller are elements of $\boldsymbol{\alpha} \in \Re^{m\times h^*}$ and $\mathbf{W} \in \Re^{h^*\times l}$.

The above equation is written in matrix form as:

$$\mathbf{F}_c^*(k) = \boldsymbol{\alpha}^* \sigma(\mathbf{W}^* \mathbf{v}) \tag{13}$$

Theoretically, the nonlinearly parameterized controller can model any sufficiently smooth function on a compact set, with arbitrarily bounded modeling error (ε_M), by a sufficiently large number of nonlinear functions (h^*). That is, for a given positive modeling error bound ε_M and a continuous function σ, there exists adaptable parameters $\boldsymbol{\alpha} = \boldsymbol{\alpha}^*$ and $\mathbf{W} = \mathbf{W}^*$, such that the output of the controller satisfies

$$\max_{V\in\Omega_v} \|\hat{\mathcal{G}}(\mathbf{v}, \boldsymbol{\alpha}, \mathbf{W}) - \bar{\mathcal{G}}(\mathbf{v})\| \leqslant \varepsilon_M \tag{14}$$

DOI: 10.1002/stc

where $\|\cdot\|$ is any suitable norm. That is,

$$\bar{\mathcal{G}}(\mathbf{v}) = \boldsymbol{\alpha}^{*}\sigma(\mathbf{W}^{*}\mathbf{v}) + \varepsilon \tag{15}$$

where $\|\varepsilon\| \leqslant \varepsilon_M$, $\boldsymbol{\alpha}^{*}$ and $\mathbf{W}^{*}$ are the ideal values of the controller parameters which are defined as,

$$(\boldsymbol{\alpha}^{*}, \mathbf{W}^{*}) := \arg \min_{(\boldsymbol{\alpha},\mathbf{W})\in\Omega_w} \left\{ \sup_{\mathbf{v}\in\Omega_v} \|\boldsymbol{\alpha}^{\mathrm{T}}\sigma(\mathbf{W}\mathbf{v}) - \bar{\mathcal{G}}(\mathbf{v})\| \right\} \tag{16}$$

in which $\Omega_w := \{(\boldsymbol{\alpha}, \mathbf{W}) | \, \|\boldsymbol{\alpha}\| \leqslant M_\alpha, \|W\|_F \leqslant M_w\}$, M_α and M_w are positive constants and $\|\ \|_F$ is Frobenius matrix norm. The Frobenius matrix norm is defined as

$$\|\mathbf{W}\|_F = tr(\mathbf{W}^{\mathrm{T}}\mathbf{W}) = \sum_{i,j} w_{ij}^2 \tag{17}$$

where $tr(\cdot)$denotes the trace of a matrix.

The value of modeling error (ε_M) depends on many factors: the type of nonlinear function (σ), the number of functions (h^{*}), elements of $\boldsymbol{\alpha}$, and $\mathbf{W}$, as well as size of compact sets Ω_v and Ω_w. Practically, the optimal parameters ($\boldsymbol{\alpha}^{*}$,$\mathbf{W}^{*}$) of the nonlinearly parameterized controller are unknown. Hence, the nonlinear function $\bar{\mathcal{G}}$ can only be approximated. The approximated adaptive control force is then given by,

$$\hat{\mathbf{F}}_c = \boldsymbol{\alpha}\sigma(\mathbf{W}\mathbf{v}) \tag{18}$$

In the following discussion, stable discrete-time parameter update laws for the controller are derived using Lyapunov method, and it will be shown that the estimated parameters remain bounded.

Discrete-time parameter update laws

By substituting the control law given by Equation (15) into Equation (6),

$$\mathbf{z}(k+1) = f_1(\boldsymbol{\xi}, k) + \mathbf{G}_1[\boldsymbol{\alpha}^{*}\sigma(\mathbf{W}^{*}\mathbf{v}) + \epsilon] + \mathbf{G}_1\mathbf{A}_g(k) \tag{19}$$

where $\boldsymbol{\xi} = (\mathbf{z}(k), \boldsymbol{\eta}(k))$. Now, substituting the approximate control law given in Equation (18) in Equation (6),

$$\hat{\mathbf{z}}(k+1) = f_1(\hat{\boldsymbol{\xi}}, k) + \mathbf{G}_1[\boldsymbol{\alpha}\sigma(\mathbf{W}\mathbf{v})] + \mathbf{G}_1\mathbf{A}_g(k) \tag{20}$$

The control objective is to ensure that $\mathbf{z}(k)$ follows a desired trajectory, $\mathbf{z}_d(k)$. The neural controller is selected such that the error between the actual and desired base structural responses is close to zero. Define error: $\mathbf{e}_b(k) = \hat{\mathbf{z}}(k) - \mathbf{z}(k)$; then, the error dynamics of the system can be written as,

$$\mathbf{e}_b(k+1) = f_1(\hat{\boldsymbol{\xi}}, k) - f_1(\boldsymbol{\xi}, k) + \mathbf{G}_1[\boldsymbol{\alpha}\sigma(\mathbf{W}\mathbf{v}) - \boldsymbol{\alpha}^{*}\sigma(\mathbf{W}^{*}\mathbf{v}) - \epsilon] \tag{21}$$

The error dynamics in Equation (21) can be written as:

$$\mathbf{e}_b(k+1) = \mathbf{A}_1\hat{\boldsymbol{\xi}}(k) - \mathbf{A}_1\boldsymbol{\xi}(k) + f_0(\hat{\boldsymbol{\xi}}, k) - f_0(\boldsymbol{\xi}, k) + \mathbf{G}_1[\boldsymbol{\alpha}\sigma(\mathbf{W}\mathbf{v}) - \boldsymbol{\alpha}^{*}\sigma(\mathbf{W}^{*}\mathbf{v}) - \epsilon] \tag{22}$$

where $f_0(\cdot)$ is the nonlinear part due to LRB system. Let the nonlinear higher order term to be $\gamma(\hat{\boldsymbol{\xi}} - \boldsymbol{\xi}) = f_0(\hat{\boldsymbol{\xi}}) - f_0(\boldsymbol{\xi})$.

Hence, the simplified error dynamics for the base can be written as,

$$\mathbf{e}_b(k+1) = \mathbf{A}_1\mathbf{e}_1(k) + \gamma(\mathbf{e}_1) + \mathbf{G}_1[\boldsymbol{\alpha}\sigma(\mathbf{W}\mathbf{v}) - \boldsymbol{\alpha}^{*}\sigma(\mathbf{W}^{*}\mathbf{v}) - \varepsilon] \tag{23}$$

where $\mathbf{e}_1 = \hat{\boldsymbol{\xi}} - \boldsymbol{\xi}$, and $\mathbf{A}_1 = f_1'|_{\hat{\xi}} = \boldsymbol{\xi}$.

Similarly,

$$\mathbf{e}_s(k+1) = \mathbf{A}_2\mathbf{e}_1(k) \tag{24}$$

where $\mathbf{A}_2 = f_2'|_0$. Combining Equations (23) and (24),

$$\mathbf{e}_1(k+1) = \bar{\mathbf{A}}\mathbf{e_1}(\mathbf{k}) + \bar{\mathbf{D}}\gamma(\mathbf{e}_1, k) + \bar{\mathbf{B}}[\boldsymbol{\alpha}\sigma(\mathbf{W}\mathbf{v}) - \boldsymbol{\alpha}^{*}\sigma(\mathbf{W}^{*}\mathbf{v}) - \varepsilon] \tag{25}$$

where $\bar{\mathbf{A}} = [f_1'|_0 f_2'|_0]^{\mathrm{T}}$, $\bar{\mathbf{D}} = [1 \ \ 0]^{\mathrm{T}}$, and $\bar{\mathbf{B}} = [\mathbf{G}_1 \ \ \mathbf{0}]^{\mathrm{T}}$. Define the parameter errors as, $\tilde{\boldsymbol{\alpha}} := \alpha - \alpha^{*}$, $\tilde{\mathbf{W}} := \mathbf{W} - \mathbf{W}^{*}$ and $\tilde{\sigma} := \sigma(\mathbf{W}\mathbf{v}) - \sigma(\mathbf{W}^{*}\mathbf{v})$, then, the error dynamics can be written as (neglecting

DOI: 10.1002/stc

the higher order terms of the form $\tilde{\boldsymbol{\alpha}}\tilde{\boldsymbol{\sigma}}$),

$$\mathbf{e}_1(k+1) = \bar{\mathbf{A}}\mathbf{e}_1(k)+\bar{\mathbf{D}}\gamma(\mathbf{e}_1,k)+\bar{\mathbf{B}}[\tilde{\boldsymbol{\alpha}}\sigma(\mathbf{W}\mathbf{v})+\boldsymbol{\alpha}\tilde{\boldsymbol{\sigma}}-\epsilon] \tag{26}$$

To facilitate the derivation of the parameter update laws, $\tilde{\sigma}$ is expanded in a Taylor series as,

$$\tilde{\sigma} = \sigma(\mathbf{W}\mathbf{v}) - \sigma(\mathbf{W}^*\mathbf{v}) = \sigma'(\mathbf{W}\mathbf{v})(\mathbf{W}-\mathbf{W}^*)\mathbf{v}+\sigma_0(\mathbf{W}\mathbf{v}) \tag{27}$$

where σ_0 are the higher order terms of the Taylor expansion, which can be written as,

$$\sigma_0(\mathbf{W}\mathbf{v}) = \sigma(\mathbf{W}\mathbf{v}) - \sigma(\mathbf{W}^*\mathbf{v}) - \sigma'(\mathbf{W}\mathbf{v})\tilde{\mathbf{W}}\mathbf{v} \tag{28}$$

The higher order terms in Equation (28) can be shown to be bounded as follows:

Using Mean-Value Theorem [24], $\exists\ \bar{\mathbf{W}} \in [\mathbf{W}, \mathbf{W}^*]$, i.e. $\bar{\mathbf{W}} = \lambda\mathbf{W}+(1-\lambda)\mathbf{W}^*$, for some $\lambda \in [0, 1]$, such that

$$\sigma_0(\mathbf{W}\mathbf{v}) = \sigma'(\mathbf{W}\mathbf{v})|_{\mathbf{W}=\bar{\mathbf{W}}}\tilde{\mathbf{W}}\mathbf{v} - \sigma'(\mathbf{W}\mathbf{v})\tilde{\mathbf{W}}\mathbf{v} \tag{29}$$

$$= [\sigma'(\mathbf{W}\mathbf{v})|_{\mathbf{W}=\bar{\mathbf{W}}} - \sigma'(\mathbf{W}\mathbf{v})]\tilde{\mathbf{W}}\mathbf{v} \tag{30}$$

Let

$$\delta := \sup_{\mathbf{v}\in\Omega_v,\ \mathbf{W}\in\Omega_w, \bar{\mathbf{W}}\in[\mathbf{W},\mathbf{W}^*]} \|\sigma'(\mathbf{W}\mathbf{v})|_{\mathbf{W}=\bar{\mathbf{W}}} - \sigma'(\mathbf{W}\mathbf{v})\| \tag{31}$$

Then, the higher order terms are bounded by,

$$|\sigma_0(\mathbf{W}\mathbf{v})| \leqslant \delta\|\tilde{\mathbf{W}}\mathbf{v}\| \tag{32}$$

By substituting $\tilde{\sigma}$ from Equation (27) into the error dynamics (Equation (26)),

$$\mathbf{e}_1(k+1) = \bar{\mathbf{A}}\mathbf{e}_1(k)+\bar{\mathbf{D}}\gamma(e_1)+\bar{\mathbf{B}}[\tilde{\boldsymbol{\alpha}}\sigma(\mathbf{W}\mathbf{v})+\boldsymbol{\alpha}\sigma'\tilde{\mathbf{W}}\mathbf{v}+\boldsymbol{\alpha}\sigma_0(\mathbf{W}\mathbf{v})-\varepsilon] \tag{33}$$

Now, the parameter update law is presented such that the overall system stability is ensured in a Lyapunov sense. It will be also shown that the NN parameters are bounded for suitably small tracking error $\mathbf{e}_1$, and hence the control inputs are bounded.

First, assume that the ANN can approximate the control law $F_c^*(k)$ given in Equation (9) with a given accuracy of ε_n, for all input $\mathbf{v}$ in a compact set.

With the above assumption, define a positive definite Lyapunov function,

$$V = \tfrac{1}{2}\left[\mathbf{e}_1(k)^{\mathrm{T}}\mathbf{P}\mathbf{e}_1(k)+tr(\tilde{\boldsymbol{\alpha}}(k)\mathbf{F}_1\tilde{\boldsymbol{\alpha}}(k)^{\mathrm{T}})+tr(\tilde{\mathbf{W}}(k)\mathbf{F}_2\tilde{\mathbf{W}}(k)^{\mathrm{T}})\right] \tag{34}$$

where $\mathbf{F}_1$ and $\mathbf{F}_2$ are constant matrices that satisfy $\mathbf{F}_1 = \mathbf{F}_1^{\mathrm{T}} > 0$ and $\mathbf{F}_2 = \mathbf{F}_2^{\mathrm{T}} > 0$. The matrix $\mathbf{P}$ is a positive-definite symmetric solution obtained from, $\bar{\mathbf{A}}^{\mathrm{T}}\mathbf{P}+\mathbf{P}\bar{\mathbf{A}} = -\mathbf{Q}$, with $\mathbf{Q}$ a positive definite matrix.

The first difference of the Lyapunov function can then be written as,

$$\Delta V = \begin{cases} -\mathbf{e}_1^{\mathrm{T}}\mathbf{Q}\mathbf{e}_1 - \mathbf{e}_1^{\mathrm{T}}\mathbf{P}\bar{\mathbf{B}}\varepsilon+\mathbf{e}_1^{\mathrm{T}}\mathbf{P}\bar{\mathbf{D}}\gamma(\mathbf{e}_1)+\mathbf{e}_1^{\mathrm{T}}\mathbf{P}\bar{\mathbf{B}}\boldsymbol{\alpha}\sigma_0(\mathbf{W}\mathbf{v}) \\ +tr\tilde{\mathbf{W}}[\mathbf{v}\mathbf{e}_1^{\mathrm{T}}\mathbf{P}^{\mathrm{T}}\bar{\mathbf{B}}\boldsymbol{\alpha}\sigma'+\mathbf{F}_2\Delta\tilde{\mathbf{W}}^{\mathrm{T}}]+tr\tilde{\boldsymbol{\alpha}}[\sigma\mathbf{e}_1^{\mathrm{T}}\mathbf{P}^{\mathrm{T}}\bar{\mathbf{B}}+\mathbf{F}_1\Delta\tilde{\boldsymbol{\alpha}}^{\mathrm{T}}] \end{cases} \tag{35}$$

Assume $\mathbf{F}_2\Delta\tilde{\mathbf{W}}^{\mathrm{T}} = -\mathbf{v}\mathbf{e}_1^{\mathrm{T}}\mathbf{P}^{\mathrm{T}}\bar{\mathbf{B}}\boldsymbol{\alpha}\sigma'$ and $\mathbf{F}_1\Delta\tilde{\boldsymbol{\alpha}}^{\mathrm{T}} = -\sigma\mathbf{e}_1^{\mathrm{T}}\mathbf{P}^{\mathrm{T}}\bar{\mathbf{B}}$. Then, the first difference of the Lyapunov function reduces to,

$$\Delta V = -\mathbf{e}_1^{\mathrm{T}}\mathbf{Q}\mathbf{e}_1 - \mathbf{e}_1^{\mathrm{T}}\mathbf{P}\bar{\mathbf{B}}\varepsilon+\mathbf{e}_1^{\mathrm{T}}\mathbf{P}\bar{\mathbf{D}}\gamma(\mathbf{e}_1)+\mathbf{e}_1^{\mathrm{T}}\mathbf{P}\bar{\mathbf{B}}\boldsymbol{\alpha}\sigma_0(\mathbf{W}\mathbf{v}) \tag{36}$$

Using the error dynamics and parameter update laws, Equation (36) can be re-written as,

$$\Delta V \leqslant \|\mathbf{e}_1\|\lambda_{\min}(\mathbf{Q})\|\mathbf{e}_1\| + \|\mathbf{e}_1\|\lambda_{\max}(\mathbf{P})\|\bar{\mathbf{B}}\|_{\mathrm{F}}\varepsilon_{\mathrm{M}} + \|\mathbf{e}_1\|\|\mathbf{P}\bar{\mathbf{D}}\|\gamma_{\mathrm{h}} + \|\mathbf{e}_1\|\lambda_{\max}(\mathbf{P})\|\bar{\mathbf{B}}\|_{\mathrm{F}}\|\boldsymbol{\alpha}\|_{\mathrm{F}}\delta \tag{37}$$

where δ is the upper bound magnitude of the higher order terms in Equation (28) and γ_h is the upper bound of magnitude error for nonlinear terms in LRB ($\gamma_h = \max(|f_0(\hat{\boldsymbol{\xi}}) - f_0(\boldsymbol{\xi})|)$.

Since the ideal parameters are constant ($\boldsymbol{\alpha}^*$, $\mathbf{W}^*$), the adaptive update laws for the parameters can be written as,

$$\boldsymbol{\alpha}(k+1)^{\mathrm{T}} = \boldsymbol{\alpha}(k)^{\mathrm{T}} - \mathbf{F}_1^{-1}\sigma\mathbf{e}_1^{\mathrm{T}}\mathbf{P}^{\mathrm{T}}\bar{\mathbf{B}} \tag{38}$$

$$\mathbf{W}(k+1)^{i\mathrm{T}} = \mathbf{W}(k)^{i\mathrm{T}} - \mathbf{F}_2^{-1}\mathbf{v}\mathbf{e}_1^{\mathrm{T}}\mathbf{P}^{\mathrm{T}}\bar{\mathbf{B}}\boldsymbol{\alpha}^i\sigma_i' \quad i = 1, 2, \ldots, h \tag{39}$$

DOI: 10.1002/stc

The error bound condition that ensures the negative semi-definiteness of the Lyapunov difference in Equation (35) can be written as,

$$\|\mathbf{e}_1\| > \frac{\lambda_{\max}(\mathbf{P})[\|\bar{\mathbf{B}}\|_F(\varepsilon_M + \|\boldsymbol{\alpha}\|_F\delta)] + \|\mathbf{P}\bar{\mathbf{D}}\|\gamma_h}{\lambda_{\min}(\mathbf{Q})} \tag{40}$$

To prevent large parameter errors, the parameters of the network are initialized offline, using finite time samples generated from an approximate model. The estimated parameters so obtained are subsequently used to begin the process of on-line adaptation.

Before proceeding further, consider Equation (21). The nonlinear terms in the equations of motion corresponding to the base are contributed by the isolation system. Specifically, the isolation forces f_x and f_y in Equations (4) and (5) consist of the un-measurable hysteretic variable $z_{x,y}$ that is the source of the nonlinearity. Here, the non-smooth signum function, *sgn* can be replaced by a smooth tanh function. It can then be verified that z_x and z_y are bounded between ± 1. For the error analysis, consider maximum value for structural system, i.e. $\|z_x\| = 1$ and $\|z_y\| = 1$. The nonlinearities in the system govern the magnitude of the bound γ_h. Since the nonlinearities are bounded, γ_h is bounded.

Hence, the error bound condition is reduced to,

$$\|\mathbf{e}_1\| > \varepsilon_a \tag{41}$$

By using Universal approximation theorem [33], it can be said that the approximation error ε_M is reduced to zero by proper selection of network architecture. It can also be shown that the higher order term δ is small and bounded. By a proper selection of the user defined matrix $\mathbf{P}$, the ratio of terms in ε_a is reduced to a small quantity.

It must be noted here that since the Lyapunov difference is negative semi-definite, the stability arguments can only be made regarding the error bounds of the system. Furthermore, by the proper selection of the user-defined matrix $\mathbf{P}$, it can be argued that the ε_a is small. If $\|\mathbf{e}_1\|$ is less than the error bound, then it will result in parameter drift. Such parameter drifts can be prevented by using projection algorithm, as discussed in [34]. The projection algorithm directs the parameters within the radius of ball Ω_w, and ensures that the parameters do not grow unbounded. Hence, the error bound conditions are satisfied.

The parameter update laws in Equations (38) and (39) require access to all the states in the system. In civil structures, full state measurements is not practical. For nonlinear systems, state estimation is cumbersome and undesirable. Hence, the update rules are approximated and specialized for the case of output feedback. Making the following substitution: $\mathbf{e}_1^{\mathrm{T}}\mathbf{P}^{\mathrm{T}}\mathbf{B} = \eta\mathbf{A}_b$, where $\mathbf{A}_b$ is the base acceleration, and η is a small scalar quantity (of the order of 10^{-2} to 10^{-4}), results in the following update laws for the parameters:

$$\boldsymbol{\alpha}(k+1)^{\mathrm{T}} = \boldsymbol{\alpha}(k)^{\mathrm{T}} - \eta\mathbf{F}_1^{-1}\sigma\mathbf{A}_b \tag{42}$$

$$\mathbf{W}(k+1)^{i\mathrm{T}} = \mathbf{W}(k)^{i\mathrm{T}} - \eta\mathbf{F}_2^{-1}\mathbf{v}\mathbf{A}_b\boldsymbol{\alpha}^i\sigma_i' \quad i = 1, 2, \ldots, h \tag{43}$$

Since the base accelerations are relatively easy to measure, the above simplified control laws (Equations (42) and (43)) allow for relatively straight-forward implementation. From the update laws in Equations (42) and (43), it can be observed that superstructure properties such as stiffness, damping and the nonlinear force terms in the isolation layer do not appear in the update laws. Hence, the controller is robust to the uncertainties in the system properties.

Controller implementation

All the simulations for this study are implemented in MATLAB [35]. The Simulink block diagram for the implementation is shown in Figure 2. The input vector $\mathbf{v}(k)$ consists of the states corresponding to the base and the ground accelerations, which are assumed to be measurable. The base acceleration response is used as the error correcting signal. The activation functions used for this network are of *tanh* type. Matrices $\mathbf{F}_1$ and $\mathbf{F}_2$ are assumed to be identity matrices. Two centralized controllers are used to control the responses in the x and y directions

DOI: 10.1002/stc

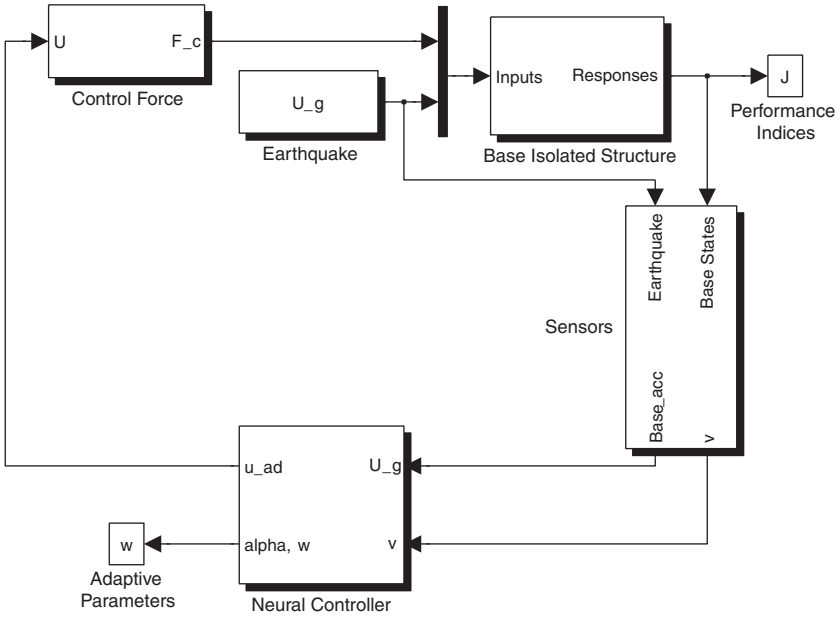

Figure 2. Simulink model for controller implementation.

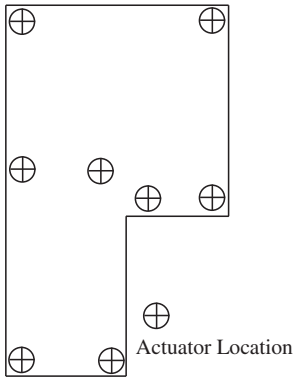

Figure 3. Actuator locations used in the numercial study.

independently. A total of 16 actuators, 8 in each direction, are distributed to the base of the structure as shown in Figure 3.

The actuator dynamics are modeled using a first-order filter of the form $K/s+t_c$, where t_c is the time constant, and K is the forward gain of the actuator. For this study t_c is assumed to be 5. Values of $t_c = 25$, 60 were investigated in this study [36]. It was then found that the maximum variation in the responses of interest was approximately 10%, and hence, only results for the case of $t_c = 5$ are reported in the next section. The actuators are assumed to saturate at 3000 kN peak force. A small random measurement noise is added (as distributed with the benchmark programs [30]) for all the simulations. The weights of the ANN are first initialized using a perturbed model of the benchmark structure. The hysteretic isolation system parameters and the structural system parameters (mass, stiffness and damping) are perturbed randomly between 5 and 15%. The perturbed model is excited using Erzinkan earthquake. The measurement noise is not added while initializing the parameters of the network. Figure 4 shows the norm of the weights ($|\Delta \mathbf{W}|$ and $|\Delta\alpha|$) as a function of the number of initialization runs (each run consists of one simulation). The initialization is stopped after the norms of the parameters stabilize, which is roughly after 120 runs.

DOI: 10.1002/stc

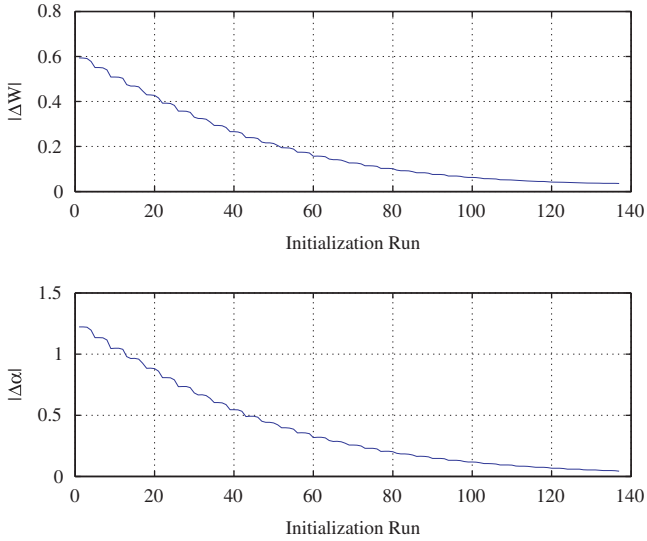

Figure 4. Parameter variation during initialization phase.

Table I. Performance indices.

Peak base shear* $J_1 = \frac{\max_t \|V_0(t)\|}{\max_t \|\hat{V}_0(t)\|}$	Peak structure shear* $J_2 = \frac{\max_t \|V_1(t)\|}{\max_t \|\hat{V}_1(t)\|}$	Peak base displacement* $J_3 = \frac{\max_t \|x_b(t)\|}{\max_t \|\hat{x}_b(t)\|}$
Peak interstory drift* $J_4 = \frac{\max_{t,f} \|d_f(t)\|}{\max_{t,f} \|\hat{d}_f(t)\|}$	Peak floor acceleration* $J_5 = \frac{\max_{t,f} \|a_f(t)\|}{\max_{t,f} \|\hat{a}_f(t)\|}$	Peak control force $J_6 = \frac{\max_t \|f_d(t)\|}{\max_t \|V_0(t)\|}$
RMS base displacement* $J_7 = \frac{\max_t \sigma_d(t)}{\max_t \hat{\sigma}_d(t)}$	RMS floor acceleration* $J_8 = \frac{\max_f \sigma_a(t)}{\max_f \sigma_{\hat{a}}(t)}$	

These performance indices were originally defined in the base-isolation benchmark study [30].
*The denominator consists of the corresponding response quantity in the uncontrolled case $f =$ floor number, 1,…,5; $t =$ time, $0 \leqslant t \leqslant T$; $\langle \cdot \rangle =$ inner product; $\| \cdot \| =$ vector magnitude; $i =$ isolator number; V_o, $V_1 =$ base and structural shears; $x_b =$ base displacement; $d_f =$ inter-story drift; $a_f =$ floor acceleration; $f_d =$ total force in the control devices; σ_d and $\sigma_a =$ RMS base displacement and floor acceleration; $W =$ Weight of the structure, 202 000 kN; $\hat{} =$ corresponding response quantity in the uncontrolled case.

SIMULATION RESULTS AND DISCUSSION

The main objective of the control design is to limit the peak isolator displacements while retaining the baseline performance of the uncontrolled base-isolated building in terms of superstructure accelerations and drifts. For this purpose, it is necessary to view the performance with respect to various quantitative measures that provide an overall measure of performance of the controller. Hence, a set of performance indices [30] as shown in Table I are used. The indices J_1 through J_5 measure the peak values of base shear, structural shear, base displacement, inter-story drift and floor accelerations, respectively. These values are normalized by their respective uncontrolled values. Uncontrolled values represent the responses of the structure when the control devices are disconnected from the structure. The performance index J_6 measures the maximum control force (normalized with respect to the peak base shear in the controlled structure) developed in the device, i.e. the peak control demand. The objective of the control design is to ensure that the values of all performance indices are as small as possible. However, in some cases, larger values of J_6 may represent low peak base shears; hence, the maximum control force is normalized with respect to the total weight of the structure and the results are included. J_7 and J_8 measure the root-mean-square (RMS) values of displacement and

DOI: 10.1002/stc

base acceleration normalized by their uncontrolled values. Readers are referred elsewhere for details [30].

The results of the controller in terms of the performance indices are presented in Table II for the nominal case. The structural responses are simulated by exciting the structure simultaneously using two components of the earthquakes (FP and FN components), as described in the benchmark paper [30]. Two sets of results are shown in Table II, which are obtained by interchanging the directions of the earthquake pairs. It can be observed from the results presented in Table II that the peak base shears (J_1) and the peak structural shears (J_2) are reduced by 40% on average compared to the uncontrolled responses. Average means an arithmetic average of the performance indices for all the earthquakes listed in Table II, for the two directions. The peak base displacements (J_3) are reduced by an average of 22%, and the maximum inter-story drifts (J_4) are reduced by an average of 32%. The average reduction in the peak floor accelerations (J_5) is approximately 27%. The RMS average displacements and accelerations (J_7 and J_8) are reduced by 34 and 32% respectively. As is evident from the results, the performance of the controller is not uniform for all the earthquakes considered. The standard deviations for peak base shear and peak structural shears are approximately 9%. The standard deviations for the base displacements, inter-story drifts and accelerations are approximately 13%. The RMS quantities have larger variations, nearly 19%. Such variability is not surprising, given that the considered structure is a nonlinear system, and the considered earthquakes have significantly different frequency characteristics and intensities. Hence, correlating the responses to a particular parameter, belonging to either the system or the excitation, is difficult.

Time-history results for Kobe and El Centro earthquakes are presented in Figures 5 and 6. The response time histories of the base acceleration, roof acceleration, base displacement and the control force are presented along with the force–displacement loops for the total isolation level force (transformed to the center of mass of the base). In order to visualize the response reductions in the superstructure, the inter-story drifts and the floor accelerations are presented in Figures 7 and 8. Except for the case of El Centro earthquake, the reductions in both the performance quantities due to the adaptive controller, namely, inter-story drifts and floor accelerations, are clearly evident. In the case of El Centro earthquake, both inter-story drifts and the floor accelerations remain close to their uncontrolled values.

These results should be viewed in the context of the overall objectives of control in base-isolated structures. In this type of structures, due to the concentration of lateral flexibility at the

Table II. Performance indices for the LRB isolation system.

Performance index	Case*	Newhall	Sylmar	El Centro	Rinaldi	Kobe	Erzinkan
J_1	Dir-1	0.670	0.502	0.717	0.715	0.515	0.565
Peak base shear	Dir-2	0.676	0.458	0.698	0.710	0.537	0.550
J_2	Dir-1	0.673	0.524	0.720	0.709	0.614	0.574
Peak structural shear	Dir-2	0.651	0.446	0.715	0.700	0.543	0.552
J_3	Dir-1	0.991	0.677	0.853	0.839	0.694	0.645
Peak base drift	Dir-2	0.991	0.608	0.841	0.918	0.716	0.626
J_4	Dir-1	0.638	0.527	0.911	0.693	0.808	0.625
Peak story drift	Dir-2	0.611	0.489	0.917	0.676	0.665	0.548
J_5	Dir-1	0.759	0.643	0.924	0.765	0.888	0.640
Peak floor acceleration	Dir-2	0.662	0.519	0.863	0.698	0.825	0.602
J_6	Dir-1	0.682	0.735	0.454	0.601	0.509	0.679
	(%W)	(8.3)	(9.4)	(3.0)	(10.3)	(3.9)	(10.0)
Peak control force	Dir-2	0.654	0.629	0.498	0.515	0.534	0.652
	(%W)	(8.2)	(8.6)	(3.1)	(8.8)	(4.3)	(9.3)
J_7	Dir-1	0.846	0.506	0.835	0.560	0.651	0.377
RMS base drift	Dir-2	0.933	0.507	0.896	0.704	0.709	0.342
J_8	Dir-1	0.789	0.543	0.875	0.687	0.807	0.437
RMS floor acceleration	Dir-2	0.793	0.463	0.910	0.618	0.846	0.381

*Uncontrolled values are equal to 1 for all performance indices, except for J_6. For J_6, $(\cdot)$ are normalized with respect to W. Dir-1 and Dir-2 refer to FP-x, FN-y, and FP-y, FN-x respectively.

DOI: 10.1002/stc

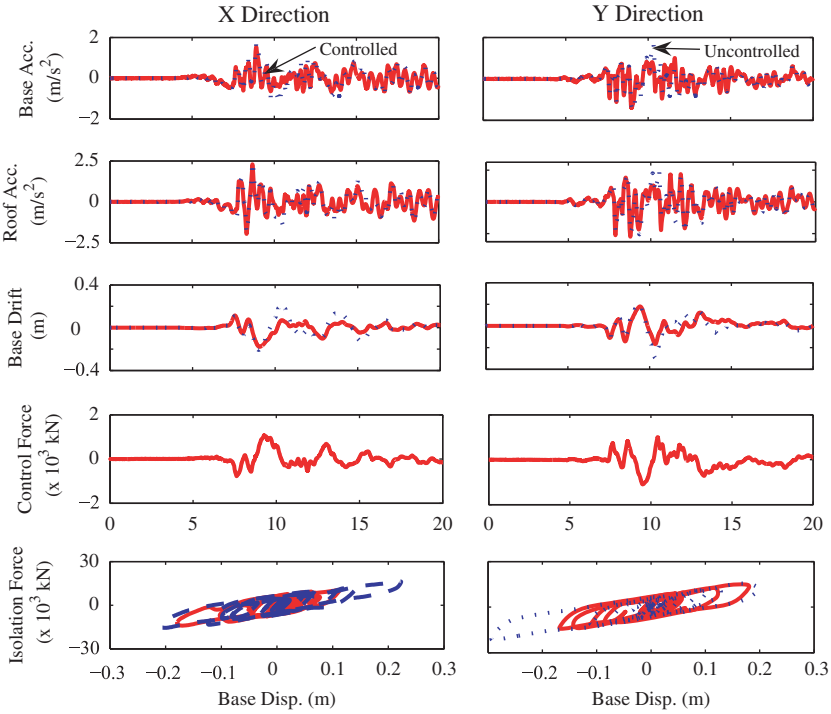

Figure 5. Results of neural controller for Kobe earthquake—Response time histories of base and roof accelerations, adaptive force commanded by the actuator at the CM of the base, and total isolation force at the center of mass of base.

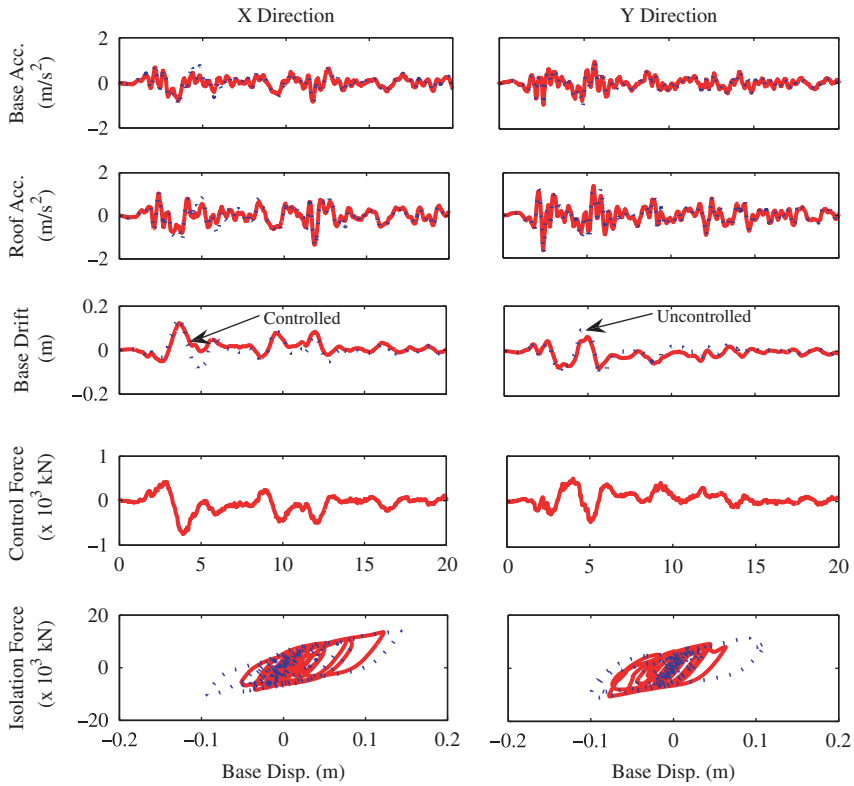

Figure 6. Results of neural controller for El Centro earthquake—Response time histories of base and roof accelerations, adaptive force commanded by the actuator at the CM of the base, and total isolation force at the center of mass of base.

DOI: 10.1002/stc

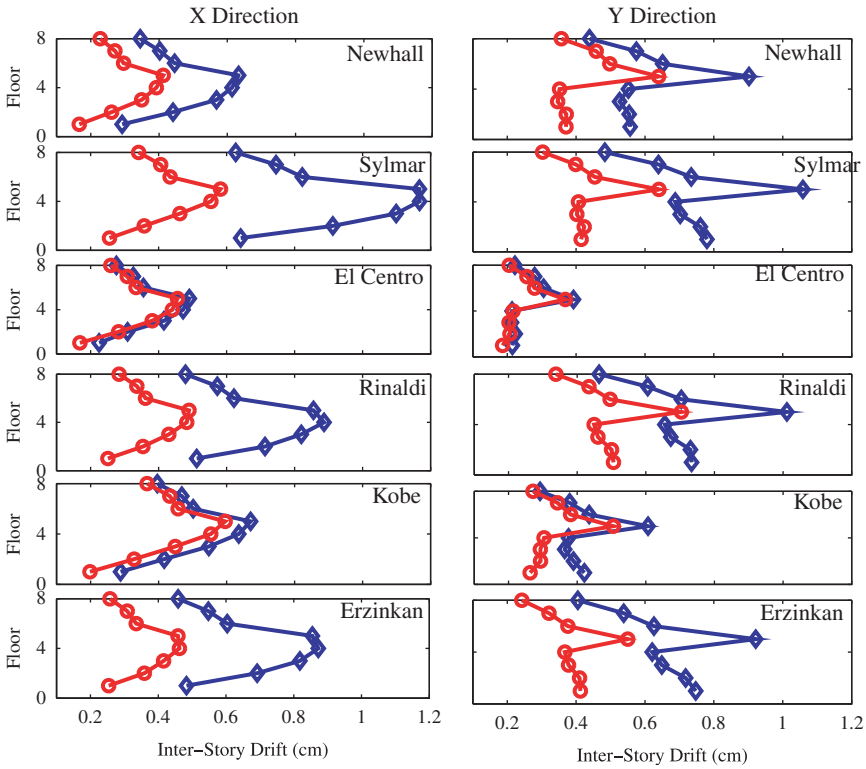

Figure 7. Results for the maximum inter-story drifts at various floors (FP-x and FN-y) for all earthquakes; controlled -o- and uncontrolled -◇-.

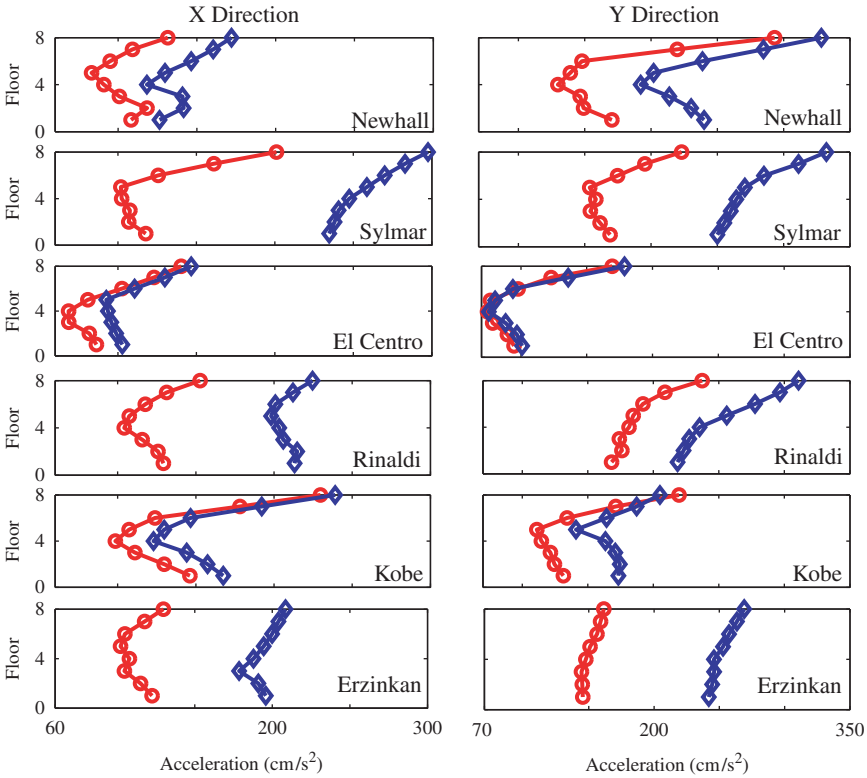

Figure 8. Results for the maximum absolute accelerations at various floors (FP-x and FN-y) for all earthquakes; controlled -o- and uncontrolled -◇-.

DOI: 10.1002/stc

isolation level, the base drifts are typically large and sometimes difficult to accommodate. This is especially the case during near-fault earthquakes and plan-irregular buildings such as the current benchmark structure under study. The primary objective of the control designs is to limit such large base drifts. Given the primary objective, it has been observed that (e.g. [6]) the superstructure drifts and accelerations increase beyond their uncontrolled values, as a result of control action at the isolation level. Increased superstructure accelerations and drifts may lead to undesirable effects in the superstructure such as increased story shears. However, in the current case, the results appear to satisfy the primary objective of reducing the base displacements, while ensuring that the superstructure drifts and floor accelerations remain below their uncontrolled values.

SUMMARY

A nonlinearly parameterized adaptive controller is presented for the active control of base-isolated structures with hysteretic isolation systems. It is shown that the adaptive controller is robust to system uncertainties and the exact representation of the nonlinear forces. Unlike popular approaches to nonlinear control, an ANN is used in the study to approximate the control law, and not the system nonlinearities, which makes it suitable to handle a wide range of nonlinearities. Adaptive parameter update laws are derived using the Lyapunov approach. By casting the problem of controlling a nonlinear base-isolated building in an adaptive framework, it is possible to derive stable parameter update laws that can achieve the performance objectives. The adaptive controller is implemented on a 3-D nonlinear base-isolated benchmark structure and the results are analyzed comprehensively. The results show that the controller is effective in reducing the base displacement of the structure without corresponding increase in the superstructure drifts and accelerations. The controller formulation, originally derived for the case of active control, can be extended to the semiactive case as well.

ACKNOWLEDGEMENTS

The authors thank the Natural Sciences and Engineering Research Council of Canada (NSERC) through their Discovery Grants Program, for the financial support to conduct this study.

REFERENCES

1. Spencer BF, Nagarajaiah S. State of the art of structural control. *Journal of Structural Engineering* (ASCE) 2003; **129**(7):845–856.
2. Yang JN, Lin S, Jabbari F. H_∞ based control strategies for civil engineering structures. *Journal of Structural Control* 2004; **10**:205–230.
3. Kelly J, Tsai HC. Seismic response of heavily damped base isolation systems. *Earthquake Engineering and Structural Dynamics* 1993; **22**:633–645.
4. Nagarajaiah S, Reinhorn AM, Constantinou MC. Nonlinear dynamic analysis of 3-d-base-isolated structures. *Journal of Structural Engineering* (ASCE) 1991; **117**(7):2035–2054.
5. Ramallo JC, Johnson E, Spencer BJ. Smart base isolation systems. *Journal of Engineering Mechanics* (ASCE) 2002; **128**(10):1088–1099.
6. Nagarajaiah S, Narasimhan S. Base isolated benchmark building part II: phase I sample controllers for linear isolation systems. *Journal of Structural Control and Health Monitoring* 2006; **13**(2):589–604.
7. Erkus B, Johnson EA. Smart base isolated benchmark building part III: a sample controller for bilinear isolation. *Journal of Structural Control and Health Monitoring* 2006; **13**(3):605–625.
8. Yang JN, Wu J, Reinhorn A, Riley M. Control of sliding-isolated buildings using sliding-mode control. *Journal of Structural Engineering* (ASCE) 1995; **122**:179–186.
9. Ikhouane F, Manosa V, Rodellar J. Adaptive control of hysteretic structural system. *Automatica* 2004; **41**:225–231.
10. Masri S, Smyth A, Chassiakos A, Caughey T, Hunter N. Application of neural networks for detection of changes in nonlinear systems. *Journal of Engineering Mechanics* 2000; **126**(7):666–676.
11. Pei J, Smyth A. New approach to designing multilayer feedforward neural network architecture for modeling nonlinear restoring forces. i: Formulation. *Journal of Engineering Mechanics* 2006; **132**(12):1290–1300.
12. Bani-Hani K, Ghaboussi J. Nonlinear structural control using neural networks. *Journal of Engineering Mechanics* 1998; **124**(2):319–327.

DOI: 10.1002/stc

13. Chen H, Tsai G, Qi J, Yang F, Amini F. Neural network for structure control. *Journal of Computing in Civil Engineering* 1995; **9**(2):168–176.
14. Ghaboussi J, Joghataie A. Active control of structures using neural networks. *Journal of Engineering Mechanics* 1995; **121**(4):555–567.
15. Liut DA, Matheu E, Singh M, Mook D. Neural-network of building structures by a force-matching training scheme. *Earthquake Engineering and Structural Dynamics* 1999; **28**:1601–1620.
16. Lee HJ, Yang G, Jung H, Spencer B, Lee, I. Semi-active neurocontrol of a base-isolated benchmark structure. *Structural Control and Health Monitoring* 2006; **13**:682–692.
17. Madan A. General approach for training back-propogation neural networks in vibration control of multi-degree of freedom structures. *Journal of Computing in Civil Engineering* (ASCE) 2006; **20**:247–260.
18. Sirca J, Adeli H. Counterpropagation neural network model for steel girder bridge structures. *Journal of Bridge Engineering* 2004; **9**(1):55–65.
19. Suresh S, Narasimhan S, Nagarajaiah S, Sundararajan N. Fault-tolerant adaptive control of nonlinear base-isolated buildings using EMRAN. *Engineering Structures* 2010; **32**(8):2477–2487.
20. Narasimhan S, Suresh S, Sundararajan N. Direct adaptive neural controller for earthquake excited nonlinear base isolated buildings. *IEEE 22nd International Symposium on Intelligent Control*, *IEEE*, Singapore, 2007; 138–143.
21. Suresh S, Narasimhan S, Sundararajan N. Adaptive control of nonlinear smart base isolated buildings using gaussian kernel functions. *Structural Control and Health Monitoring* 2007; **15**(4):585–603.
22. Narasimhan S. Robust direct adaptive controller for the nonlinear highway bridge benchmark. *Structural Control and Health Monitoring* 2009;**16**(6):599–612.
23. Ioannou PA, Fidan B. *Adaptive Control Tutorial*. SIAM: Philadelphia, 2006.
24. Astrom K, Wittenmark B. *Adaptive Control*. Addison-Wesley Publishing Company: New York, 1995.
25. Narendra KS. Neural networks for control: theory and practice. *Proceedings of the IEEE* 1996; **84**(10):1385–1406.
26. Calise AJ, Rysdyk RT. Nonlinear adaptive flight control using neural networks. *IEEE Control Systems Magazine* 1998; **18**(6):14–25.
27. Sanner RM, Slotine JE. Gaussian networks for direct adaptive control. *IEEE Transactions on Neural Networks* 1992; **3**(6):837–863.
28. Luo N, Rodellar J, Sen DL, Vehi J. Output feedback sliding mode control of base isolated structures. *Journal of the Franklin Institute* 2000; **337**:555–577.
29. Pozo F, Ikhouane F, Pujol G, Rodellar J. Adaptive backstepping control of hysteretic base-isolated structures. *Journal of the Vibration and Control* 2006; **12**(4):373–394.
30. Narasimhan S, Nagarajaiah S, Gavin H, Johnson EA. Base isolated benchmark building part I: problem definition. *Journal of Structural Control and Health Monitoring* 2006; **13**(2):573–588.
31. Leontaritis IJ, Billings SA. Input-output paramteric models for non-linear systems part i: deterministic non-linear systems. *International Journal of Control* 1985; **41**(2):303–328.
32. Suresh S, Omkar S, Mani V, Sundararajan S. Direct adaptive neural flight controller for f-8 fighter aircraft. *Journal of Guidance*, *Control*, *and Dynamics* 2006; **29**(2):454–464.
33. Haykin S. *Neural Networks*: *A Comprehensive Foundation*. Prentice-Hall, Inc.: New Jersey, 1999.
34. Goodwin GC, Mayne DQ. A parameter estimation perspective of continuous time model reference adaptive control. *Automatica* 1987; **23**:57–70.
35. MATLAB. The Math Works, Inc.: Natick, Massachusetts, 2000.
36. Dyke SJ, Spencer B, Quast P, Sain MK. The role of control-structure interaction in protective system design. *Journal of Engineering Mechanics* (ASCE) 1995; **121**(2):322–338.

DOI: 10.1002/stc